Electronic Supplementary Information

Mechanisms of controlled stabilizer-free synthesis of gold nanoparticles in liquid aerosol containing plasma

Jaehyun Nam[1], Gaurav Nayak[1], Stephen Exarhos[1], Chelsea M. Mueller[2], Dongxuan Xu[1], George Schatz[2] and Peter J Bruggeman[1]

Experimental methods

Plasma reactor

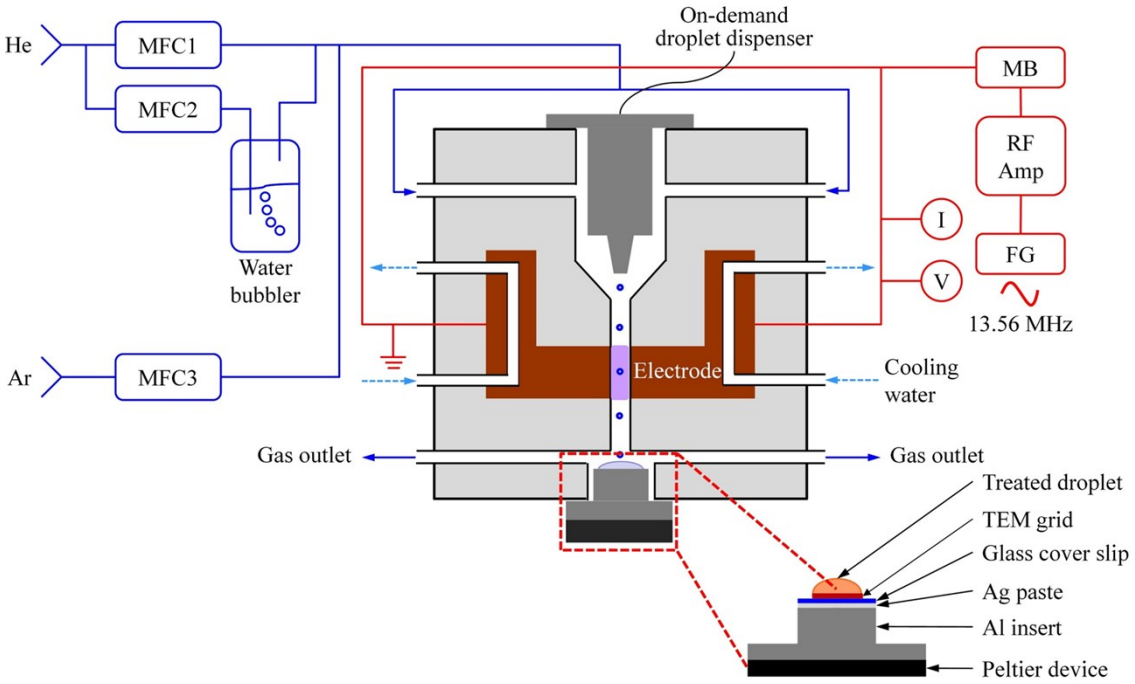

Figure S1. Schematic of the plasma-droplet reactor used for the synthesis of AuNPs.

Figure S1 shows a schematic of the plasma-droplet reactor used in this work. This reactor has previously been used for the study of the formate decomposition in plasma-treated droplets [1], [2] and for the gas-phase diagnostics of helium and argon plasmas [3], [4]. In brief, an atmospheric pressure RF-driven capacitively coupled glow discharge was generated between two water-cooled copper parallel plate electrodes with an inter-electrode spacing of 2 mm and an electrode cross-sectional area of 19.1 × 9.5 mm^2. An admixture of 17% Ar and 17% Ar + 0.2% H_2O in He were used. The addition of Ar is motivated

by the ability to assess VUV emission effects with a MgF_2 window as shown in Nayak et al [5]. The discharge power was calculated as described in [6], and kept constant at ~6 W for He/Ar plasma and varied between 6 and 14 W for He/Ar/H_2O plasma. The operating power was limited by the constriction of the plasma at elevated powers, enhanced by the presence of liquid droplets.

Droplet generation, collection and characterization

The liquid precursor droplets were generated by an on-demand micro-droplet dispenser (MicroFab Technologies Inc. MJ-ATP-01-070) mounted on the top of the plasma reactor as shown in **Figure** S1. The dispenser produces droplets with a diameter of 41 ± 2 µm at frequencies of 200 and 1600 Hz using a piezoelectric force actuated by tailored waveform control (MicroFab Technologies Inc. JetDrive™ III CT-M5-01). The droplets were carried with the feed gas through the plasma region on to the droplet collector cooled by a Peltier device for analysis. The droplet size and dynamics were captured by microscopic imaging using a fast framing camera (Photron FASTCAM Mini UX50) and analyzed as described in [1]. The total flow rate of the feed gas varied between 1 and 3 standard liters per minute (slm).

For AuNP synthesis, a 1 mM gold(III) chloride trihydrate ($HAuCl_4.3H_2O$) aqueous solution was prepared from a solid powder (Sigma-Aldrich) dissolved in high purity deionized water (HPLC-grade) at room temperature. The plasma treated as well as unprocessed droplets (dispensed but no plasma) were collected at the bottom of the plasma reactor on a glass cover slip (Bellco, 5 mm). For TEM analysis, the droplets were directly collected on a 300-mesh copper TEM grid (Ted Pella, Inc.) mounted on top of the glass cover slip for ~2.5 min. For absorption measurements of the plasmonic resonance of the AuNPs, the droplets were collected and frozen on impact to reduce further inherent reactions within the collected droplets or via plasma afterglow, on the glass cover slip cooled with a Peltier device for ~10 min in two runs to obtain a volume of 20 µl. This volume was further diluted in water to obtain a final volume of 150 µl (7.5 times dilution). UV-vis absorption spectroscopy was performed in a micro quartz cuvette with an absorption path length of 1 cm with a deuterium + tungsten lamp (Avantes AvaLight-DH-CAL) as the light source and a broadband spectrometer (Avantes AvaSpec-2048) as the detector. The procedure for the collection of plasma-treated droplets for absorption measurements might vary due to the uneven changes in the evaporation rate of the droplets for different operating conditions and the small deviation in the treatment time to collect 20 µl of the treated droplets. Due to this uncertainty, we have avoided discerning any pattern in the absorbance curves (as a function of flow rate or discharge power), but only considered binary comparisons, i.e., if there is significant absorbance or not. All measurements were performed with HPLC grade distilled water as the reference solution.

TEM was performed on a Tecnai T12 instrument with LaB6 source and 120 kV accelerating voltage. For each sample, at least 10 TEM images were taken. The images included in the figures in this section were selected as the most representative of each sample's composition. Due to the harsh grid preparation conditions, some TEM grids were partially damaged. In these cases, additional spots were identified on the grids to ensure the acquired images appropriately represented the sample character. There were no cases in which a TEM grid was totally unusable after preparation.

The NP size distributions were generated manually from select representative TEM images using the Measure function in ImageJ. In these size distributions, particles are assumed to be spherical, although

they do not always appear spherical in the TEM images. Sizes of non-spherical particles were assigned by taking an approximate mean diameter. In some images, very small particles (1-3 nm) were difficult to distinguish from the background. In these instances, a threshold was imposed on the image in ImageJ at a level such that no background artifacts were found above the threshold. Contrast was enhanced based on this threshold to make the small particles clearly distinguishable. When possible, >100 particles were measured to ensure reasonable precision. Size distributions with n > 75 particles were fitted with lognormal distributions. The mean particle size and standard deviation were calculated from the obtained best fit results. For images with n < 75 particles, no lognormal distribution was superimposed. Mean size and standard deviation in these cases were calculated assuming a random distribution of particle sizes.

The gold ion complexes composition depend on the pH of solution, and our precursor solution was acidic, pH ~3, so the precursor was present in the form of $AuCl_4^-$. The concentration of $AuCl_4^-$ was measured with UV-vis absorption spectroscopy at ~300 nm which exhibits an absorption feature due to the ligand metal charge transfer band [7], [8]. However, we observed that the peak at 300 nm is impacted by a contribution of absorption in the presence of AuNPs. Therefore, the treated solutions were processed with a centrifuge (Thermo Scientific mySPIN 12 Mini) with 12,500 rpm for more than 30 minutes to allow for separating AuNPs from the solution. We collected a 20-30 μL of solution volume (10 minutes plasma treatment) followed by 5 times of dilution, ~100-150 μL as a result, before analysis of the samples was performed. To consider the effect of evaporation on the concentration of treated samples, the ratio between the actual volume collected and the theoretical volume dispensed was calculated, and the ratio was multiplied to the absorbance profiles as a correction factor. Three cases for each condition (treated by He/Ar or He/Ar/H_2O) were measured and the final absorbance profiles were averaged. The precursor solution of 0.2 mM (5 times dilution) yields an absorbance of ~ 0.47 at 300 nm before treatment. For the He/Ar plasma treated sample, after the treatment and centrifugation, the absorbance at 300 nm was reduced to 0.07. Using the Beer-Lambert law, the ratio of remaining concentration to the initial concentration of $AuCl_4^-$, yields the remaining percentage of ion precursors and allows to calculate the amount of converted $AuCl_4^-$.

AuNP synthesis control measurements

As control experiments, solutions of water containing 1 mM $HAuCl_4.3H_2O$ were treated with 1 ml of 3.6 mM and 34.3 mM H_2O_2 for a period of 3.75 and 5 min, respectively. These concentrations were chosen because these corresponded to the concentration of H_2O_2 formed in plasma treated droplets for 3.75 min and 5 min, respectively (see H_2O_2 **measurement**). For the TEM analysis, 5 µl of this solution was dropped on a 300-mesh Cu TEM grid. For NP absorption measurements, a similar procedure was followed as described previously.

To evaluate the effect of long-lived reactive species, such as H_2O_2, on AuNP synthesis, a droplet with a volume of 15 µl containing Au precursor solution placed at the bottom of the reactor was treated with the plasma afterglow (He/Ar at 6 W for 3.75 min, and He/Ar/H_2O at 14 W for 5 min) at a total gas flow rate of 2 slm. The afterglow-treated droplet was characterized using both UV-vis absorption and TEM analysis. To account for the increase in volume (15 to 85 µl) of the droplets used in the control

measurements, the treatment time with the plasma effluent was also proportionally increased to 21 (He/Ar) and 28 (He/Ar/H_2O) minutes.

Local electron properties measurement

Continuum radiation was used to determine the global (spatially averaged across the inter-electrode gap) and the local (near the location of the droplet with minimum optical emission intensity of continuum radiation) electron density and temperature in the absence and presence of droplets, respectively. This was achieved by recording absolute broadband emission spectra and subsequent analysis of the bremsstrahlung as described in detail in [1], [3].

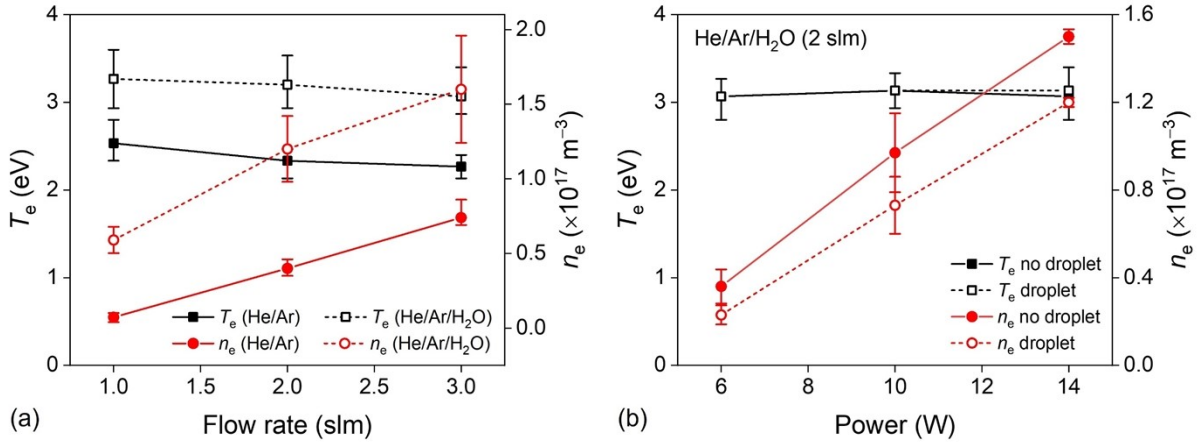

Figure S2. Local electron properties determined from the continuum radiation measurements in (a) He/Ar and He/Ar/H_2O plasmas operated at 6 W and 14 W, respectively, in the presence of droplets (1600 Hz) as a function of gas flow rate at the location of the droplet, and (b) He/Ar/H_2O plasma operated at 2 slm in the presence (1600 Hz) and absence of droplets as a function of plasma power.

H_2O_2 measurement

Since H_2O_2 is proven to be an effective reducing agent for Au^{3+}, we measured the H_2O_2 concentrations in the water droplet with or without gold precursor treated at different plasma conditions. The dissolved H_2O_2 concentrations in the plasma-treated droplets were measured by a colorimetric method using titanium oxysulfate ($TiOSO_4$) as the reagent as described in [9]. The droplets were collected and frozen on impact on the glass cover slip at the bottom of the reactor for a period of 3.75 min (He/Ar plasma at ~6 W) and 5 min (He/Ar/H_2O plasma at ~14 W). Two different treatment times were used due to different rates of evaporation in He/Ar and He/Ar/H_2O plasmas to obtain a final liquid volume of 10 µl, which was then diluted in 90 µl of distilled water and 100 µl of $TiOSO_4$. The procedure is described in detail in [10]. The absorbance of the resulting solution was determined at 405 nm using a broadband spectrometer (Avantes AvaSpec-2048) and an LED (Thorlabs M405LP1) as the light source. The concentration was deduced from a calibration procedure with a detection limit of 100 µM.

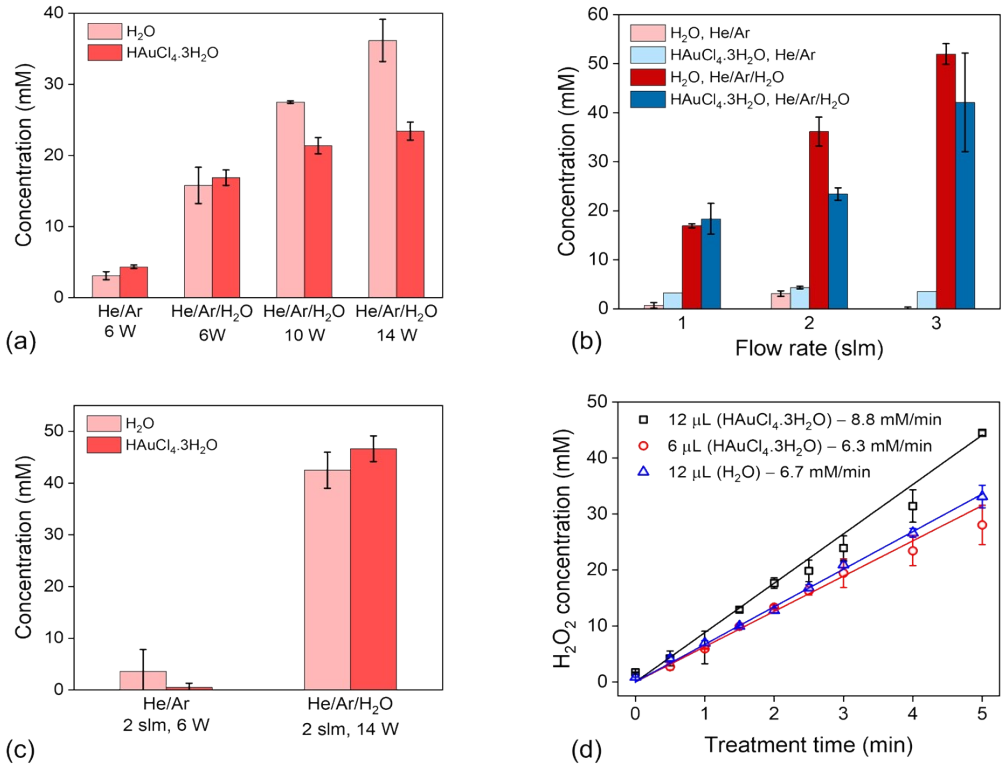

Figure S3. Measured H_2O_2 concentrations in different experimental conditions. (a) H_2O_2 measured in plasma-treated droplets containing H_2O and 1 mM $HAuCl_4.3H_2O$ in He/Ar and He/Ar/H_2O plasmas as a function of power at 2 slm. (b) H_2O_2 measured in plasma-treated droplets containing H_2O and 1 mM $HAuCl_4.3H_2O$ in He/Ar (6 W) and He/Ar/H_2O (14 W) plasmas as a function of gas flow rate. (c) H_2O_2 measured in a droplet of volume 10 µl containing H_2O and 1 mM $HAuCl_4.3H_2O$ placed at the bottom of the reactor and treated with the plasma afterglow at 2 slm. (d) H_2O_2 measured in a drop containing H_2O and 1 mM $HAuCl_4.3H_2O$ placed at the bottom of the reactor and treated with the plasma afterglow (He/Ar/H_2O at 14 W and 2 slm).

We measured H_2O_2 concentrations of a few tens of mM in the droplet treated by H_2O-containing plasma, much more than in droplets treated with He/Ar plasma, as shown in **Figure S2**. The H_2O_2 concentration increases with plasma power monotonously for droplets without added Au precursor, however, it saturates in droplets containing Au precursor solution after 6 W as shown in **Figure S2 (a)**. The measured H_2O_2 concentrations from precursor contained droplets treated by He/Ar/H_2O plasma did not strongly depend on the plasma power (**Figure S2 (a))** but increased significantly with increasing gas flow rate (**Figure S2 (b))**. To explain this finding, the H_2O_2 concentrations were also measured in droplets placed at the bottom of the reactor treated with the plasma afterglow as shown in **Figure S2 (c)**. In He/Ar/H_2O plasma at 14 W, the measured H_2O_2 concentrations in plasma-treated and afterglow-processed H_2O droplets are similar (~40 mM), while the H_2O_2 concentrations are almost twice larger in the afterglow-treated drops containing Au precursor solution compared to direct plasma-treated droplets. This suggests that the majority of the measured H_2O_2 is due to afterglow treatment of collected droplets at the bottom of the reactor for He/Ar/H_2O plasma. For instance, in the afterglow treatment of drops with He/Ar/H_2O plasma (2 slm, 14 W and 5 min), an average H_2O_2 concentration of 45 mM is measured (**Figure S2 (c)**), and a linear increase in H_2O_2 concentration is observed with treatment time as shown in

Figure S2 (d). Regarding the average afterglow treatment time of droplets collected on the bottom is 2.5 min, it suggests that a H_2O_2 concentration of at least 22.5 mM can be accumulated in the collected droplets in the afterglow, which is very similar to the H_2O_2 concentration measured from collected droplets containing Au precursor dispensed through the plasma.

Conversion of precursor ions

To calculate the percentage conversion of precursor ions, the ratio of absorbance of measured sample (A_{300}) to the precursor solution (A_{300}') at 300 nm was multiplied by the volume ratio between the collected sample (V) and theoretical volume dispensed (V_{th}). The theoretical volume dispensed was calculated by the droplet volume (determined from the fast imaging [5]) and dispensing frequency. This is to adjust the ion concentration which could be elevated by the evaporation by the plasma treatment. Each case consists of three repeated measurements. The samples were diluted 5 times to avoid saturation of the absorbance.

Table S1 Detailed calculations of conversion based on UV-vis absorbance data. A_{300}/A_{300}' denotes the ratio of absorbance at 300 nm between the measured sample and precursor (5 times diluted). V/V_{th} denotes the ratio between actual volume of samples collected and theoretical volume dispensed.

	He/Ar, 6W			He/Ar/H_2O, 12W		
	1	2	3	1	2	3
$\frac{A_{300}}{A_{300}'}$	0.20	0.06	0.20	0.17	0.40	0.53
$\frac{V}{V_{th}}$	0.62	0.81	0.74	0.55	0.53	0.45
$\frac{A_{300}}{A_{300}'} \times \frac{V}{V_{th}}$	0.13	0.05	0.15	0.09	0.21	0.23
Conversion (%)	87	95	85	91	79	77
Mean $\pm$ Std (%)	89 ± 5			72 ± 8		

1-D Diffusion model

The diffusion model assumes much faster reduction of precursor ions at the droplet interface compared to transport timescales so that the concentration of ions at the plasma-droplet interface can be approximated as zero. The equation solved numerically is as follows:

$$r^2 \frac{\partial C_{Au^{3+}}}{\partial t} = \frac{\partial}{\partial r}\left(D_{Au^{3+}} r^2 \frac{\partial C_{Au^{3+}}}{\partial r}\right) \quad (1)$$

For the plasma treatment time in the experiment (~10 ms), the distribution of $AuCl_4^-$ is shown in **Figure**

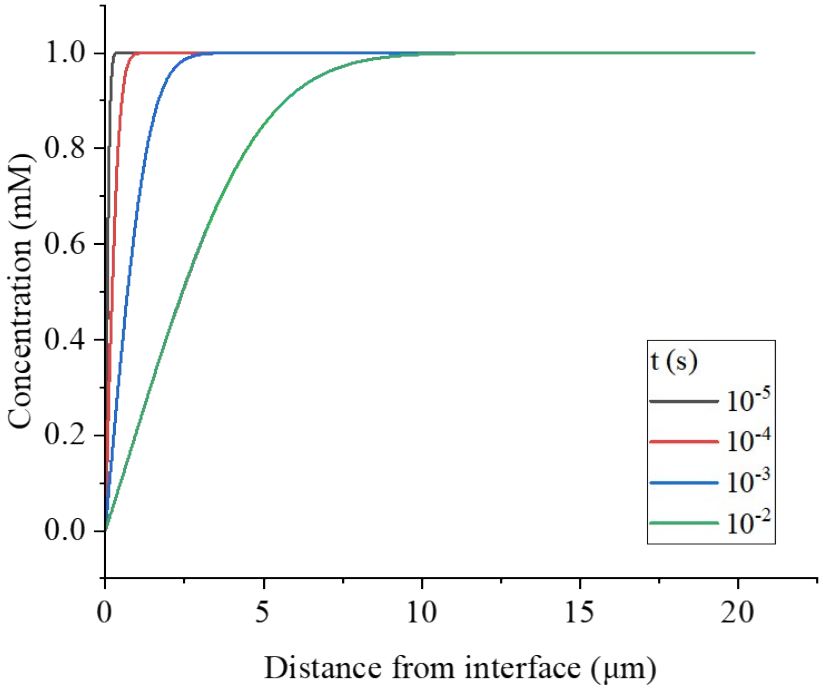

Figure S4. Precursor ion ( ) spatial distribution as obtained from the diffusion model for different times during the plasma exposure of the droplet.

S3. Note that the reported diffusion coefficient of $AuCl_4^-$ is $5 \times 10^{-10} m^2/s$ [11]. The time integral of the converted $AuCl_4^-$ concentration during 10 ms was 0.27 mM. As the calculation yields an upper limit of conversion due to interfacial reactions, this result suggests the maximum percentage conversion during the plasma enabled by short-lived plasma-produced species is 27%.

1-D reaction-diffusion model

The reduction mechanism considered for the model is as follows:

$$Au^{3+} + 3R \rightarrow Au^0 \qquad 2$$

where R denotes a reducing species including e_{aq}^- and other possible other short-lived species such as H radicals produced through vacuum UV photolysis. The reaction is assumed to only occur at the plasma-droplet interface and be sufficiently fast so the reaction is transported limited (see further) as has been shown to be a good approximation for plasma-induced conversion of organic molecules in droplets [5].

The rate equation of nucleation over supersaturation ($S > 1$) is expressed as below:

$$R_{nu} = A\, exp\left(-\frac{16\pi\gamma^3 v_0^2}{3k_B^3 T^3 (lnS)^2}\right) \quad (3)$$

where $R_{nu}, \gamma, v_0, k_B, T, A,$ and S are the rate of nucleation, surface free energy per unit area, atomic volume, Boltzmann's coefficient, temperature of solution, pre-exponential factor, and the degree of supersaturation. The pre-exponential factor A is expressed as

$$A = \frac{4k_B T}{9\eta v_0} C_{Au^0} \quad (4)$$

where η and C_{Au^0} denote dynamic viscosity of the solvent and the concentration of the monomer, respectively [12]. The degree of supersaturation is a dimensionless number expressed by

$$S = \frac{C_{Au^0}}{C'_{Au^0}} \quad (5)$$

where C'_{Au^0} is the solubility of monomers. Although the solubility and surface free energy per unit area of gold monomers in water solution are not exactly known, Chen et al [12] used their model to fit these parameters to the experiments. Their calculated parameters ($C'_{Au^0} = 4 \times 10^{-7}\, M, \gamma = 205\, mN/m$) fit the experimental results and explained the results from the Vaia [13] and Polte [14] groups as well. In addition to this work, the lowest $HAuCl_4$ concentration used for AuNP synthesis in plasma-liquid system reported in the literature is $10\ \mu M$ [15] which sets the upper limit of solubility. To calculate the rate of AuNP formation from nucleation, we assume that after nucleation, gold clusters are formed with the smallest amount of gold atoms corresponding to a magic-numbered gold cluster corresponding to a stable icosahedral shape. The magic number M_N corresponding to the number of gold atoms and the radius R_N of magic-numbered cluster are expressed as [16]

$$M_N = \frac{1}{3}(2n+1)(5n^2+5n+3) \quad (6)$$

$$R_N = (2n+1) r_{AuNP} \quad (7)$$

where n is an integer and r_{Au} is the radius of gold atom. Hence, we assume that all nuclei are composed of 13 atoms ($n = 1, M_N = 13$), and the rate of nucleating monomers ($R_{nu,\ Au^0}$) is expressed as

$$R_{nu,\ Au^0} = -13 R_{nu}. \quad (8)$$

Furthermore, we assume that particle growth is dominantly caused by diffusion-limited absorption of monomers and autocatalytic surface growth facilitated by H_2O_2. The rate constant of diffusion-limited absorption of monomers onto a nucleus is expressed by the Smoluchowski relation [17]:

$$k_d = 4\pi D_{rel} R C_{rel} \quad (9)$$

where $D_{rel}, R, and\ C_{rel}$ are the relative diffusion coefficient, encounter distance, and relative bulk concentration of monomers, respectively. We assume that the size of NP is much larger than the size of monomers and the concentration of NP is much smaller than the density of monomers. Therefore,

$D_{rel} \cong D_{Au^0}$, $C_{rel} \cong C_{Au^0}$, and $R \cong R_{NP}$, where R_{NP} is approximated by the radius of the NP. The rate of diffusion-limited absorption of monomers ($\dot{R}_d$) is then expressed as:

$$\dot{R}_d = k_d C_{NP} = 4\pi D_{Au^0} R_{AuNP} C_{AuNP} C_{Au^0}. \quad (10)$$

Complex gold ions ($AuCl_4^-$) are consumed by autocatalytic surface growth of NPs expressed by mechanism **R3**, and the rate of autocatalytic surface growth ($\dot{R}_{AC}$) is expressed as

$$\dot{R}_{AC} = k_{AC} C_{AuCl_4^-} (C_{AuCl_4^-,0} - C_{AuCl_4^-}) \quad (11)$$

where $C_{Au^{3+},0}$ is the initial concentration of precursor ions. From the calculation of Meader et al [18], the dependency between the rate constant of autocatalytic surface growth, k_{AC}, and $C_{H_2O_2}$ was $k_{AC} \sim (C_{H_2O_2})^{1/2}$ rather than $k_{AC} \sim (C_{H_2O_2})^{3/2}$ as shown in reaction **R3**. The concentration of H_2O_2 was kept constant as 34.3 mM, which is the measured H_2O_2 concentration of the plasma treated droplet (He/Ar/H_2O plasma at 14 W), throughout the simulation. We tested this simplifying assumption and regardless of the evolution of the H_2O_2 concentration in a droplet, the simulation results were mainly sensitive to the final concentration of H_2O_2 (see **Modeling H_2O_2 concentration**).

The rate of diffusion-limited absorption of monomers depends on the size of NP hence we need to calculate the radius of NP during the growth process. We assume that all particles can be described by an average size. The average number of gold atoms in each NP (M_{mean}) hence can be expressed as:

$$M_{mean} = \frac{N_d + N_{AC}}{N_{NP}} + 13 \quad (12)$$

where N_{NP}, N_d and N_{AC} denote the number of AuNPs, consumed gold monomers for diffusion-absorption and autocatalytic surface growth, respectively. The second term on the right-hand side is due to the nuclei size which are composed of 13 atoms. The time-derivative form of Eq.14 is calculated by a first-order differential equation:

$$\frac{dM_{mean}}{dt} = \frac{(\dot{N}_d + \dot{N}_{AC})}{N_{NP}} - \frac{N_d + N_{AC}}{N_{NP}^2} \dot{N}_{NP} = \frac{(\dot{N}_d + \dot{N}_{AC})}{N_{NP}} - \frac{M_{mean} - 13}{N_{NP}} \dot{N}_{NP} = \frac{\iiint (\dot{R}_d + \dot{R}_{AC}) dV}{\iiint C_{NP} dV} - \frac{M_{mean} - 13}{\iiint (C_{NP}) dV} \quad (13)$$

From M_{mean} and the icosahedral structure of gold (Eqs. 6 and 7), the mean particle radius (R_{NP}) can be determined. Reaction-diffusion equations are listed as below:

$$r^2 \frac{\partial C_{Au^{3+}}}{\partial t} = \frac{\partial}{\partial r}\left(D_{Au^{3+}} r^2 \frac{\partial C_{Au^{3+}}}{\partial r} \right) - r^2 \dot{R}_{AC} \quad (14)$$

$$r^2 \frac{\partial C_{Au^0}}{\partial t} = \frac{\partial}{\partial r}\left(D_{Au^0} r^2 \frac{\partial C_{Au^0}}{\partial r} \right) - r^2 \left(\dot{R}_{nu,\,Au^0} + \dot{R}_d \right) \quad (15)$$

$$r^2 \frac{\partial C_{NP}}{\partial t} = \frac{\partial}{\partial r}\left(D_{NP} r^2 \frac{\partial C_{NP}}{\partial r} \right) + r^2 \dot{R}_{nu} \quad (16)$$

We implement the concept of reducing current Γ_R which is a total current of short-lived species such as solvated electrons and H produced by photolysis. As reported by Maguire et al [19], and as shown

earlier in this work, the short timescale of AuNP synthesis implies a very fast reduction process. In addition, the exact mechanism and kinetics of reduction are still unknown. Therefore, we assume short-lived species quickly reduces Au^{3+} into Au^{0} at the interface. This approach allows to include the reduction as a boundary condition for which the balance of the outward flux of Au^{3+} and the inward flux of Au^{0} can be expressed by the reducing boundary flux as:

$$g_{Au^{3+}} = -g_{Au^{0}} = -\frac{1}{3}g_R \qquad 17$$

where g denotes a species flux. Note that the species current is defined by $\Gamma = \int g \cdot ds = 4\pi g R_p^2$. The boundary condition in Eq. 17 is only applied within the droplet residence time in the plasma volume. We furthermore limit the current to maintain $C_{Au^{3+}} \geq 0\ mM$ at the plasma-droplet interface. We used COMSOL Multiphysics partial differential equation module for the computation.

Modeling H_2O_2 concentration

The H_2O_2 concentration produced by afterglow treatment of collected droplets will follow linear increase as shown in the manuscript. Therefore, the actual temporal evolution of H_2O_2, combination of plasma exposure and afterglow treatment effect, will lie between two limiting cases, constant H_2O_2 throughout simulation and linear increase with the slope shown in **Figure S2** (d). From our investigation, we observed that the two limiting cases showed negligible differences in the simulation outcome (~2 % and < 0.1% differences in the number of atoms and diameter of AuNP, respectively). Therefore, the concentration of H_2O_2 is kept constant as 34.3 mM throughout the simulation.

Estimation of AuNP concentration

The concentration of AuNPs can be estimated based on the measured particle diameter and estimated conversion of the precursor ions. As reported in the manuscript at least 70% of gold ions are reduced, corresponding to a conversion of at least 0.7 mM in the droplet. The measured particle diameter treated by He/Ar/H_2O plasma is between 5-16 nm. According to the icosahedral nanoparticle model [16], 5-16 nm AuNPs will have atoms between 2000 – 70,000. Therefore, if we divide converted ions of 0.7 mM – 1 mM with 2000 – 70,000 per particle, the concentration of AuNPs is between $7 \times 10^{-6} mM - 5 \times 10^{-4} mM$.

Effect of H_2O_2 concentration to the particle size

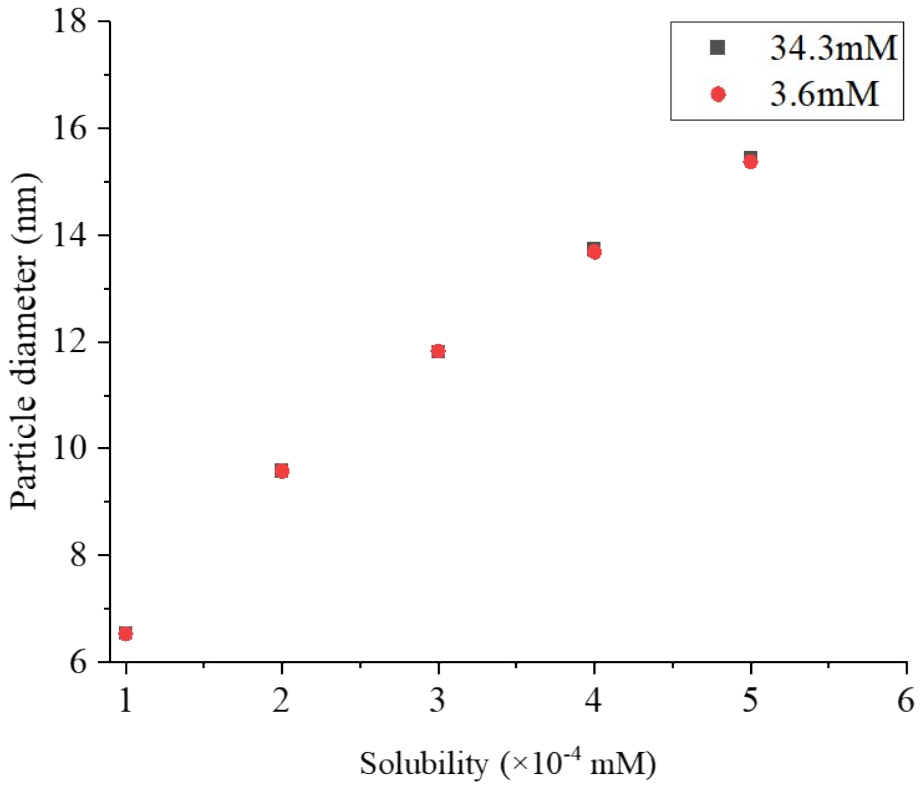

Figure S5. The diameter of AuNP from simulation by different H_2O_2 concentration (34.3mM and 3.6mM) at .

In the manuscript, we argued that a much lower H_2O_2 concentration in the droplets treated by He/Ar 6W than He/Ar/H_2O plasma was attributed as a candidate for causing the smaller size in the droplets treated by He/Ar 6W plasma. To investigate this, we ran simulations with two different H_2O_2 concentrations (34.3mM and 3.6mM) measured from afterglow treatment of precursor solution. The size difference caused by different H_2O_2 concentrations is shown in **Figure S4**, where negligible difference is observed. The percentage of size reduction was less than 0.2% on average. This is because, due to the much longer timescale of simulation (or droplet collection) than that of autocatalytic surface reaction (2-3 orders of magnitude longer), the autocatalytic surface growth is limited by the concentration of gold ions in the solution ($< 1\ mM$), not by the concentration of H_2O_2 ($> 3\ mM$).

References

[1] G. Nayak, G. Oinuma, Y. Yue, J. S. Sousa, and P. Bruggeman, "Plasma-droplet interaction study to assess transport limitations and the role of·OH, O·, H·, O2 (a 1Δ g), O3, He (23 S) and Ar (1s 5) in formate decomposition," *Plasma Sources Science and Technology*, vol. 30, no. 11, p. 115003, 2021.

[2] G. Oinuma, G. Nayak, Y. Du, and P. J. Bruggeman, "Controlled plasma-droplet interactions: A quantitative study of OH transfer in plasma-liquid interaction," *Plasma Sources Science and Technology*, vol. 29, no. 9, 2020, doi: 10.1088/1361-6595/aba988.

[3] G. Nayak, M. Simeni Simeni, J. Rosato, N. Sadeghi, and P. J. Bruggeman, "Characterization of an RF-driven argon plasma at atmospheric pressure using broadband absorption and optical emission spectroscopy," *Journal of Applied Physics*, vol. 128, no. 24, p. 243302, 2020.

[4] G. Nayak, N. Sadeghi, and P. J. Bruggeman, "He(23S1) and He2(a3Σu+) metastables densities measured in an RF-driven helium plasma using broadband absorption spectroscopy," *Plasma Sources Science and Technology*, vol. 28, no. 12, p. 125006, Dec. 2019, doi: 10.1088/1361-6595/ab3691.

[5] G. Nayak, J. Wang, R. Li, D. Aranzales, S. M. Thagard, and P. J. Bruggeman, "Non-OH-driven liquid-phase chemistry in water microdroplets," *Plasma Processes and Polymers*, vol. n/a, no. n/a, p. e2200222, doi: 10.1002/ppap.202200222.

[6] S. Hofmann, A. F. H. Van Gessel, T. Verreycken, and P. Bruggeman, "Power dissipation, gas temperatures and electron densities of cold atmospheric pressure helium and argon {RF} plasma jets," *Plasma Sources Science and Technology*, vol. 20, no. 6, p. 65010, 2011.

[7] H. B. Gray, "Electronic Structures of Square Planar Metal Complexes," in *Proceedings of the 8th International Conference on Coordination Chemistry*, V. Gutmann, Ed., Vienna: Springer, 1964, pp. 133–135. doi: 10.1007/978-3-7091-3650-8_46.

[8] R. P. Briñas, M. Hu, L. Qian, E. S. Lymar, and J. F. Hainfeld, "Gold Nanoparticle Size Controlled by Polymeric Au(I) Thiolate Precursor Size," *J. Am. Chem. Soc.*, vol. 130, no. 3, pp. 975–982, Jan. 2008, doi: 10.1021/ja076333e.

[9] G. Eisenberg, "Colorimetric Determination of Hydrogen Peroxide," *Ind. Eng. Chem. Anal. Ed.*, vol. 15, no. 5, pp. 327–328, May 1943, doi: 10.1021/i560117a011.

[10] G. Nayak *et al.*, "Rapid inactivation of airborne porcine reproductive and respiratory syndrome virus using an atmospheric pressure air plasma," *Plasma Processes and Polymers*, vol. 17, no. 10, p. 1900269, Oct. 2020, doi: 10.1002/ppap.201900269.

[11] M. B. Hariri, A. Dolati, and R. S. Moakhar, "The Potentiostatic Electrodeposition of Gold Nanowire/Nanotube in HAuCl4 Solutions Based on the Model of Recessed Cylindrical Ultramicroelectrode Array," *J. Electrochem. Soc.*, vol. 160, no. 6, p. D279, Apr. 2013, doi: 10.1149/2.141306jes.

[12] X. Chen, J. Schröder, S. Hauschild, S. Rosenfeldt, M. Dulle, and S. Förster, "Simultaneous SAXS/WAXS/UV–Vis Study of the Nucleation and Growth of Nanoparticles: A Test of Classical Nucleation Theory," *Langmuir*, vol. 31, no. 42, pp. 11678–11691, Oct. 2015, doi: 10.1021/acs.langmuir.5b02759.

[13] H. Koerner, R. I. MacCuspie, K. Park, and R. A. Vaia, “In Situ UV/Vis, SAXS, and TEM Study of Single-Phase Gold Nanoparticle Growth,” *Chem. Mater.*, vol. 24, no. 6, pp. 981–995, Mar. 2012, doi: 10.1021/cm202633v.

[14] J. Polte *et al.*, “Mechanism of Gold Nanoparticle Formation in the Classical Citrate Synthesis Method Derived from Coupled In Situ XANES and SAXS Evaluation,” *J. Am. Chem. Soc.*, vol. 132, no. 4, pp. 1296–1301, Feb. 2010, doi: 10.1021/ja906506j.

[15] N. Shirai, S. Uchida, and F. Tochikubo, “Synthesis of metal nanoparticles by dual plasma electrolysis using atmospheric dc glow discharge in contact with liquid,” *Japanese Journal of Applied Physics*, vol. 53, no. 4, p. 46202, 2014.

[16] T. Mori and T. Hegmann, “Determining the composition of gold nanoparticles: a compilation of shapes, sizes, and calculations using geometric considerations,” *J Nanopart Res*, vol. 18, no. 10, p. 295, Oct. 2016, doi: 10.1007/s11051-016-3587-7.

[17] M. Smoluchowski, “Mathematical theory of the kinetics of the coagulation of colloidal solutions,” *Z. Phys. Chem*, vol. 92, pp. 129–168, 1917.

[18] V. K. Meader, M. G. John, C. J. Rodrigues, and K. M. Tibbetts, “Roles of Free Electrons and H2O2 in the Optical Breakdown-Induced Photochemical Reduction of Aqueous [AuCl4]−,” *J. Phys. Chem. A*, vol. 121, no. 36, pp. 6742–6754, Sep. 2017, doi: 10.1021/acs.jpca.7b05370.

[19] P. Maguire *et al.*, “Continuous In-Flight Synthesis for On-Demand Delivery of Ligand-Free Colloidal Gold Nanoparticles,” *Nano Lett.*, vol. 17, pp. 1336–1343, 2017, doi: 10.1021/acs.nanolett.6b03440.